Article

Acid-Catalyzed Etherification of Glycerol with *Tert*-Butanol: Reaction Monitoring through a Complete Identification of the Produced Alkyl Ethers

Alfonso Cornejo [1,2], Inés Reyero [1,2], Idoia Campo [1], Gurutze Arzamendi [1,2] and Luis M. Gandía [1,2,*]

[1] Departamento de Ciencias, Universidad Pública de Navarra (UPNA), 31006 Pamplona, Spain; alfonso.cornejo@unavarra.es (A.C.); ines.reyero@unavarra.es (I.R.); icampoaran@educacion.navarra.es (I.C.); garzamendi@unavarra.es (G.A.)

[2] Institute for Advanced Materials and Mathematics (InaMat2), Universidad Pública de Navarra (UPNA), 31006 Pamplona, Spain

[*] Correspondence: lgandia@unavarra.es

Abstract: Higher *tert*-Butyl glycerol ethers (*t*BGEs) are interesting glycerol derivatives that can be produced from *tert*-butyl alcohol (TBA) and glycerol using an acid catalyst. Glycerol *tert*-butylation is a complex reaction that leads to the formation of five *t*BGEs (two monoethers, two diethers, and one triether). In order to gain insight into the reaction progress, the present work reports on the monitoring of glycerol etherification with TBA and *p*-toluensulfonic acid (PTSA) as homogeneous catalysts. Two analytical techniques were used: gas chromatography (GC), which constitutes the benchmark method, and ^{1}H nuclear magnetic resonance (^{1}H NMR), whose use for this purpose has not been reported to date. A method for the quantitative analysis of *t*BGEs and glycerol based on ^{1}H NMR is presented that greatly reduced the analysis time and relative error compared with GC-based methods. The combined use of both techniques allowed for a complete quantitative and qualitative description of the glycerol *tert*-butylation progress. The set of experimental results collected showed the influence of the catalyst concentration and TBA/glycerol ratio on the etherification reaction and evidenced the intrinsic difficulties of this process to achieve high selectivities and yields to the triether.

Keywords: etherification; glycerol; homogeneous acid catalyst; reaction monitoring; *tert*-butylation

1. Introduction

Glycerol is currently produced in large amounts as a byproduct of the biodiesel industry. According to ChemAnalyst the global glycerol market was about 1 million tons in 2021, and it is expected to grow at a compound annual rate of 4.5% until 2030. The personal care, cosmetic, and pharmaceutical industry sectors dominate this demand [1]. On the other hand, the production of glycerol associated to biodiesel is much higher. Indeed, according to the International Energy Agency [2], 45,712 million liters of biodiesel were produced in 2021, which allows estimating the biodiesel production at about 40.2 million tons (assuming a mean biodiesel density of 0.88 g/cm^3) and that of glycerol in crude (non-refined) form at 4.4 million tons. Therefore, there is great interest in developing new uses capable of absorbing the surplus in order to improve the economic balance of the biodiesel production processes and introducing that sustainable resource in the value chain, thus contributing to the circular economy.

Since the large-scale emergence of biodiesel as an alternative fuel, some 25 years ago, many review papers have appeared reporting on the progress made in the methodss for transforming glycerol into value-added products. Referring to some of the recent studies, Morais Lima et al. [3] described the production of propylene glycol, acrolein, epichloro-hydrin, dioxalane, dioxane, and glycerol carbonate through chemical routes and that of 1,3-propanediol, *n*-butanol, citric acid, ethanol, butanol, propionic acid, mono-, di-, and

triacylglycerols, cynamoil esters, glycerol acetate, and benzoic acid by means of biochemical processes, mainly enzymatic. Checa et al. [4] discussed the rational formulation of the catalysts required depending on the chemistry of the transformation route according to reforming (steam and aqueous phase), hydrogenolysis, reduction, selective oxidation, and acetalization reactions. Direct uses of crude glycerol and recent valorization approaches such as the production of alkyl-aromatics and activated carbon were also highlighted. Other important conversion processes were dehydration, pyrolysis, gasification, selective trans-esterification, etherification, fermentation, oligomerization, and polymerization [5]. Kaur et al. [6] emphasized the environmental advantages of the biological conversion of crude glycerol and included among the valuable products polyglycerols, polyhydroxyalkanoates, solketal, trehalose, and various organic acids (lactic, glyceric, succinic, docosahexaenoic, and eicosapentaenoic). A recently proposed and very promising route of glycerol valorization is its catalytic deoxygenation for (bio)olefin (e.g., propylene) production [7]. The plethora of possible products that can be obtained from glycerol illustrates its frequent designation as a platform chemical.

There is also big interest in the applications of glycerol as a fuel (through combustion) and as a source of fuels (e.g., hydrogen, biogas, syngas, and ethanol) and fuel additives [5,8,9]. Fuel additives are commonly used in order to improve thermal engines performance, reduce their pollutant emissions, and modify specific physicochemical properties of commercial gasoline, diesel, and biodiesel. Oxygenated derivatives of glycerol such as ethers, acetals, and esters (acetates) have been reported as fuel additives [10,11]. The *tert*-butyl glycerol ethers (*t*BGEs) resulting from the reaction between isobutylene or *tert*-butanol and glycerol are precisely of particular interest as concerns the present work. Depending on the number of hydroxyl groups of the glycerol molecule that become alkylated, this reaction, also known as glycerol *tert*-butylation (see Figure 1), leads to the formation of two monoether isomers (*t*B1GE-a and *t*B1GE-b), two diether isomers (*t*B2GE-a and *t*B2GE-b), and a triether (*t*B3GE). Due to the limited solubility of the monoethers in the most common fuels, the products preferred as additives are the diethers and, especially, the triether. The *t*BGEs have been found to increase the octane number of gasoline and have been claimed as substitutes for methyl and ethyl *tert*-butyl ethers (MTBE and ETBE, respectively). When used as diesel and biodiesel additives, the main positive effects of *t*BGEs are the reduction in particulate matter and soot emissions [11]. On the other hand, alkylated glycerol monoethers have interesting surfactant and biological properties and find application as components of cosmetics and personal care and pharmaceutical products [12–14].

Glycerol etherification reactions have been thoroughly reviewed by Palanychamy et al. [15]. Glycerol *tert*-butylation involves three consecutive and reversible steps, leading to the successive formation of *tert*-butyl glycerol mono-, di-, and triethers (see Figure 1). The reaction is typically carried out in the presence of strong acid catalysts, and when *tert*-butanol (*tert*-butyl alcohol, TBA) is used as the alkylating agent, each step is accompanied by the liberation of a water molecule. Much of the early work on this field has been performed reacting glycerol and isobutylene (isobutene, 2-methylpropene, IB); a commercial process was developed based on this synthetic route [16]. IB requires operating the reactor under pressure (around 20 atm) in order to keep the olefin in the liquid state, although it is immiscible with glycerol, thus leading to a heterogeneous reaction system characterized by mass transport limitations [16,17]. These features, and the possibility of IB oligomerization to form diisobutylenes as side reaction, have been considered disadvantages that have encouraged the use of TBA instead of IB in more recent works. Nevertheless, the presence of coproduced water has been found to negatively affect the acid catalysts and introduce thermodynamic limitations that introduce thermodynamic limitations that make more complex reaching high yields of the higher (di-, and specially, tri-) *t*BGEs with TBA than with IB [18]. As for the catalysts required, homogeneous acids, i.e., those that are soluble in glycerol, such as *p*-toluensulfonic acid or the heteropoly acid $H_3PW_{12}O_{40}$, are much more active than the heterogeneous ones and allow obtaining significantly higher yields of

di- and tri-*t*BGEs [16]. The interest in avoiding the use of the homogeneous acids due to corrosion, safety, and environmental issues has fostered the search for solid acid catalysts among which cation exchange resins with highly crosslinked structure, large pore zeolites, sulfonated mesostructured silicas and carbons, and supported tungstophosphoric acid have provided the best results with both IB [19–25] and TBA [19,26–32]. These materials require a fine-tuning of their acid and textural properties in order to develop suitable catalytic activity and selectivity toward higher *t*BGEs; at the same time, they are also very sensitive to water, which solvates the hydrophilic active sites, rendering them poorly active.
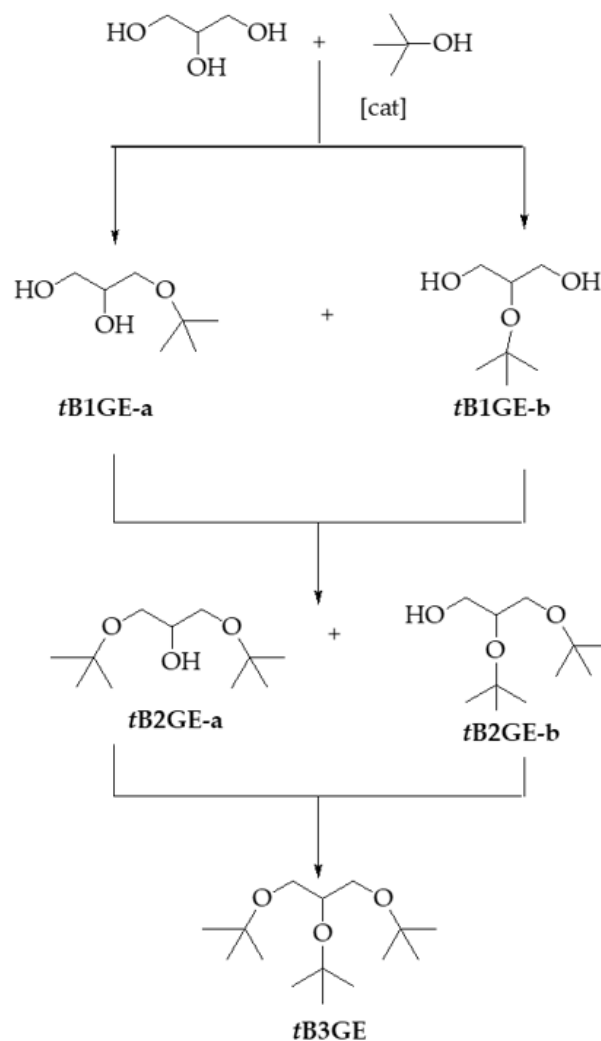

Figure 1. Products of the glycerol *tert*-butylation reaction with indication of the nomenclature used to refer to the several *tert*-butyl glycerol ethers.

In the vast majority of glycerol *tert*-butylation reports available, it is customary to lump the isomers as monoethers and diethers, and even the diethers and triether are sometimes lumped as higher ethers. In the present work, procedures for the identification and analysis of the different *tert*-butyl glycerol ethers are presented. The five *t*BGEs were obtained in our laboratories, isolated, and completely characterized by HRMS-ESI+, ATR-FT-IR, and NMR. A straightforward methodology is presented that allows for fast and reliable monitoring of the reaction between glycerol and *tert*-butanol (TBA) catalyzed with *p*-toluensulfonic acid (PTSA) combining ^{1}H NMR and conventional GC-FID analyses. It is expected this way to contribute to a complete characterization of the reacting system, as well as providing an improved description of the steps involved in the *tert*-butylation reaction.

Gas chromatography (GC) is the benchmark technique for the quantitative analysis of *t*BGEs; however, except made of *t*B1GE-a, the *t*BGEs are not easily available, which complicates the equipment calibration. Melero et al. [20,33] proposed to extrapolate the response factor obtained for *t*B1GE-a to the higher ethers. Other authors determined the response factors for all the individual ethers after column chromatography separation and purification from the reaction mixture [23,24,34], which is quite laborious.

Nuclear magnetic resonance (NMR) has become in recent years a high-throughput analytical technique for the characterization of complex mixtures. This is the case, for example, of the monitoring and/or quantitative analysis of reaction mixtures from the digestion of woody biomass [35–38], lignin depolymerization [39], or transesterification reaction for biodiesel production [40,41]. However, the purification of tertiary mono and di *tert*-butyl glycerol ethers is elusive, and to the best of our knowledge, their characterization has not been reported to date. As for the secondary mono and di-*tert*-butyl glycerol ethers and tri-*tert*-butyl glycerol ether, their NMR spectra have been reported [42–44]. Nevertheless, descriptions are, in some cases, imprecise when providing the chemical shifts for the ^{1}H NMR [44] or simplistic when explaining the spin systems of etherification products [42]. Indeed, the chemical shifts reported by Jamróz et al. [44], which describe the spin system, and those reported by González et al. [42] corresponding either to the glycerol skeleton hydrogen atoms or to the methyl groups in the *tert*-butyl moieties did not match at all between them.

2. Results and Discussion

2.1. Characterization of Etherification Products

The five *tert*-butyl ethers of glycerol were synthetized as indicated in the Materials and Methods Section 3.3. After their isolation and purification, the corresponding chemical structure and expected formula were confirmed by NMR and ESI[+] (see Figure A1). Glycerol and di- and tri-*tert*-butyl ethers presented the expected $[M + Na]^+$ as the major peak (*m/z* 227.1613 for *t*B2GE-a, *m/z* 227.1626 for *t*B2GE-b, and *m/z* 283.2267 for *t*B3GE). This peak was accompanied by $2M + Na^+$ in the case of *t*B2GE-a. More reactive monoethers presented the peak corresponding to $[M + Na]^+$ (*m/z* 171.0996). Condensation of the primary hydroxyl groups was observed under the ESI[+] analysis conditions for *t*B1GE. Thus, in the case of *t*B1GE-a, *m/z* 301.1988 was detected after the condensation of two molecules under the analysis conditions, producing $[2M-H_2O + Na]^+$. *t*B1GE-b presented an additional primary hydroxyl group, and in addition to $[M + Na]^+$ (*m/z* 171.0996), the major peak appeared at *m/z* 413.2647, which corresponds to $[3M-3H_2O + Na^+]$ as a result of the higher reactivity of these primary hydroxyl groups, due to their lower steric hindrance, to become a crown-ether like structure under the analysis conditions.

ATR-FT-IR spectra of the isolated compounds showed the gradual disappearance of the hydroxyl O–H stretching band at ca. 3400 cm^{-1} as the degree of etherification increased accompanied by the intensification of the aliphatic bands between 2974 and 2834 cm^{-1} that correspond to the C–H stretching mode (see Figure A2). As expected, no major differences were observed between *t*B2GE-a and *t*B2GE-b with this technique.

As for the NMR spectra, Table 1 gathers the chemical shifts and coupling constant for the hydrogen atoms on the glycerol skeleton that are identified in Figure 2. Given the symmetry of *t*B1GE-b, *t*B2GE-a, and *t*B3GE, the ^{1}H NMR signals were easier to assign (see Figures A5, A7 and A11). In contrast, the secondary C_2 carbon of *t*B1GE-a and *t*B2GE-b was asymmetric, and therefore, C_1 was diasterotopic, which complicated the interpretation of their ^{1}H NMR spectra (see Figures A3 and A9). The hydrogen atoms on the glycerol skeleton of *t*B1GE-a appeared as a set of three ^{1}H NMR signals in the range from 3.42 ppm to 3.81 ppm (see Figure 3a), whereas both hydroxyl hydrogen atoms appeared as broad shoulders at 2.40 ppm. As expected, the *tert*-butyl moiety appeared as a singlet at 1.19 ppm. The assignation of H and C signals was performed using ^{13}C APT and HMBC correlation. The ^{1}H signal at 1.19 ppm from –C–CH_3 presented long-range correlation with the quaternary C atom at 73.66 ppm (see Figure 3b). These signals also presented

long-range correlation with the signal of H_1 centered at 3.43 ppm, which also correlated with C_3 at 63.92 ppm in the HMBC spectrum (see Figure 3b). C_2 is a chiral center; therefore, both H_1 and H_3 are diasterotopic. Hence, they appeared as a set of two signals each (H_{1a} and H_{1b}; H_{3a} and H_{3b}) with large geminal coupling constants, JH_{1a}-H_{1b} = 9.1 Hz and JH_{3a}-H_{3b} = 11.4 Hz. The coupling constants with H_2 were in the 3.9–5.8 Hz range. Because of the coupling with the non-equivalent H_1 and H_3 atoms, the ^1H NMR signals for H_2 were shown as multiplet centered at 3.78 ppm. The ^1H NMR spectra of tB1GE-a could be satisfactorily simulated using WINDNMR [45].

Table 1. Chemical shifts and coupling constant for the hydrogen atoms on the glycerol skeleton of the *t*BGEs as identified in Figure 2.

Ether	H_{1a} $(J_{1a,2})$	H_{1b} $(J_{1b,2})$	$(J_{1a,1b})$	H_2	H_{3a} $(J_{3a,2})$	H_{3b} $(J_{3b,2})$	$(J_{3a,3b})$	C_1–OC $[CH_3]_3$	C_2–OC $[CH_3]_3$	C_3–OC $[CH_3]_3$
*t*B1GE-a	3.43 (5.88)	3.49 (3.92)	(9.10)	3.78	3.65 (4.95)	3.70 (3.91)	(11.4)	1.20	-	-
*t*B1GE-b	3.65	-	-	3.71	3.65 [a]	-	-	1.24	-	-
*t*B2GE-a	3.37 (5.92)	3.42 (5.06)	(8.97)	3.78	3.37 [a] (5.92) [a]	3.42 [b] (5.06) [b]	(8.98)	1.19	-	1.19
*t*B2GE-b	3.34 (8.58)	3.41 (4.30)	(8.62)	3.65	3.61	3.61	-	1.21	1.19	-
*t*B3GE	3.27 (5.32)	3.37 (5.92)	(9.22)	3.60	3.27 [a] (5.32) [a]	3.37 [b] (5.92) [b]	(9.22) [a,b]	1.17	1.20	1.17

[a] Symmetry H-1a and H-3a. [b] Symmetry H-1b and H-3b.
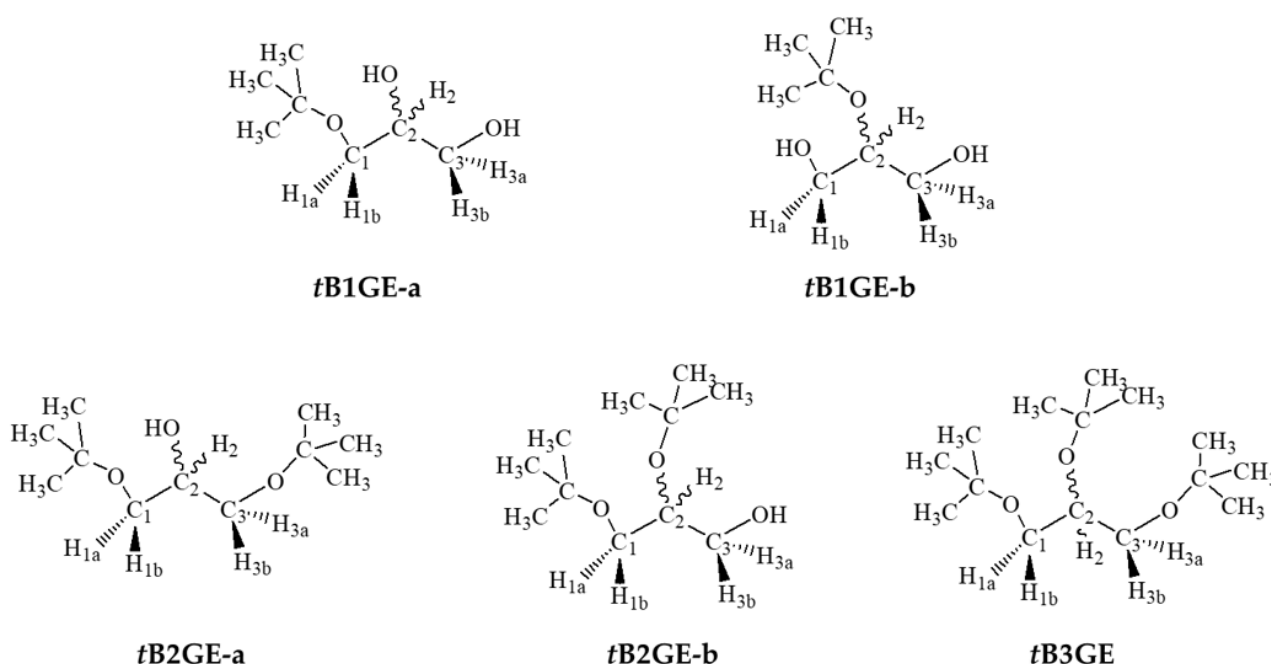

Figure 2. Identification of the hydrogen and carbon atoms on the glycerol skeleton of the *t*BGEs for ^1H NMR chemical shift assignment (see Table 1).
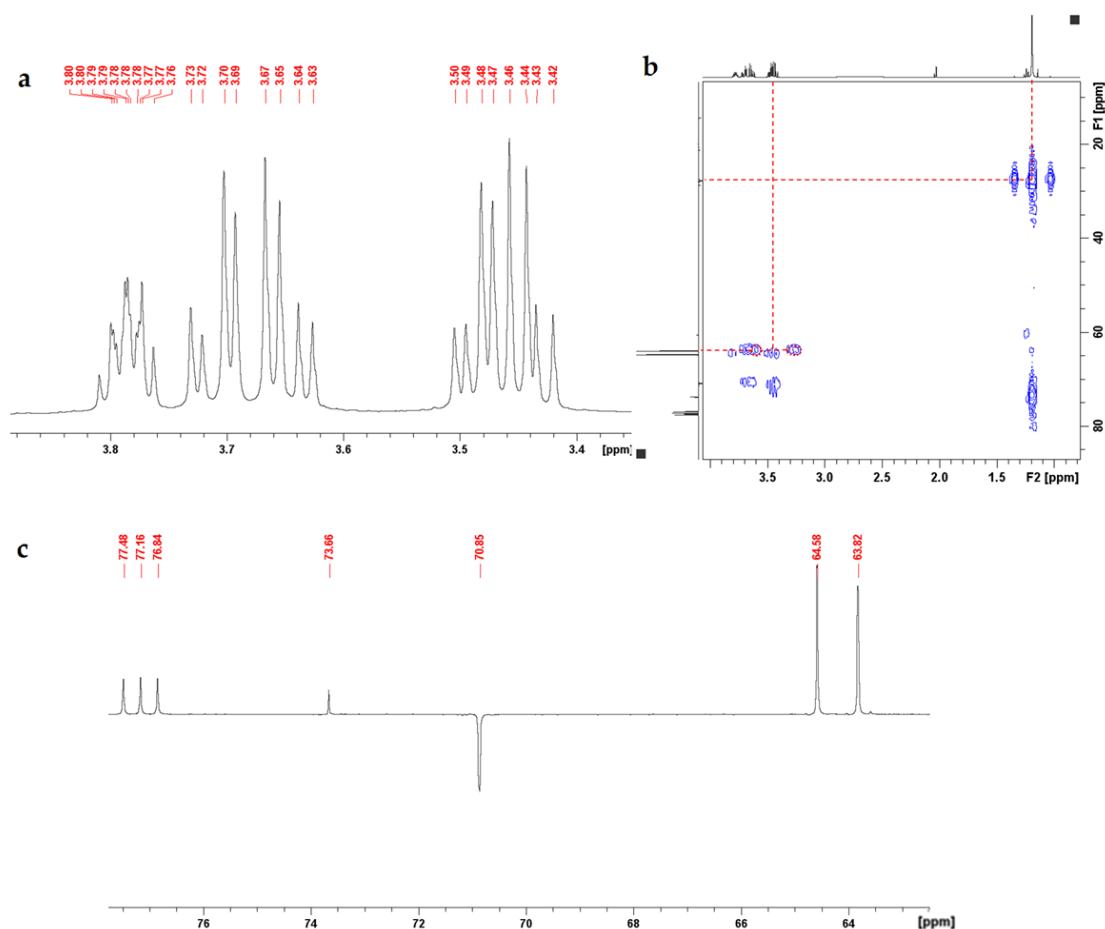
Figure 3. Details of *t*B1GE-a spectra: (**a**) ^{1}H NMR spectrum in the 3.35–3.85 ppm region, (**b**) HMBC experiment, and (**c**) ^{13}C APT spectrum.

Analysis of the spectra for symmetric *t*B2GE-a and tB3GE was much simpler. In the case of *t*B2GE-a, the ^{1}H NMR spectrum showed the signal of the hydrogen atom on the *tert*-butyl group as a singlet at 1.19 ppm, whereas the signal corresponding to the hydroxyl group appeared as a doublet at 2.54 ppm (J = 4.48 Hz). The signal for H_2 appeared as a hexuplet centered at 3.78 ppm showing an apparent coupling constant of 5.27 Hz. Because of the symmetry of the molecule, H_1 and H_3 were equivalent and turned out a unique signal at 3.39 ppm. However, as in the case of *t*B1GE-a, H_a and H_b presented slightly different chemical shifts because of their diasterotopic character. Indeed, nuclei $H_{1a,3a}$ and $H_{1b,3b}$ showed slightly different chemical shifts of 3.37 ppm and 3.42 ppm, respectively, with a large geminal coupling constant of J_{ab} = 8.97 Hz being J_{a2} = 5.92 Hz and J_{b2} = 5.06 Hz. Therefore, the signal for H_2 centered at 3.78 ppm actually corresponded to a triple triplet with J_{a2} = 5.92 Hz and J_{b2} = 5.06 Hz but could not be accurately resolved. The ^{13}C APT spectrum (Figure 3c) allowed the easy assignation of carbon atom signals, as indicated in Table 2.

The ^{1}H NMR spectrum of tB3GE presented a similar pattern to that of *t*B2GE-a. H_{1a} and H_{3a} appeared at 3.27 ppm, showing large coupling constants with H_{1b} and H_{3b}, J_{ab} = 9.22 Hz, and J_{a2} = 5.32 Hz, whereas H_{1b} and H_{3b} appeared at 3.37 ppm with J_{b2} = 5.92 Hz. The similarity for the J_2 coupling constants suggested that H_2 had the appearance of a well-defined quintuplet whose apparent coupling constant (J = 5.57 Hz) averaged J_{a2} and J_{b2}. The ^{13}C APT spectra for *t*B2GE-a and *t*B3GE were far simpler and allowed easier identification of the corresponding signals (see Appendix B). In the case of *t*B2GE-a, the signal at 27.52 ppm was attributed to the primary methyl groups on the *tert*-butyl moieties, the signal at 72.99 ppm to the quaternary carbon on the *tert*-butyl

moieties, and that at 62.9 ppm to the secondary C_1 and C_3. Similarly, for tB3GE, the HMBC spectrum showed long-range correlations between the hydrogen signal at 1.17 ppm and the quaternary C atom at 72.56 ppm, as well as the hydrogen signal at 1.20 ppm and the quaternary C atom at 73.68 ppm, allowing the assignation of these quaternary C atoms.

Table 2. Chemical shifts for the carbon atoms of the tBGEs.

Ether	C_1	C_1–O–C–(CH₃)₃ [a]	C_1–O–C–(CH₃)₃ [a]	C_2	C_2–O–C–(CH₃)₃ [a]	C_2–O–C–(CH₃)₃ [a]	C_3
tB1GE-a	63.92	27.59	73.69	70.80	-	-	64.69
tB1GE-b	63.83	-	-	71.12	28.68	74.75	63.83
tB2GE-a	63.09	27.70	73.17	70.38	-	-	63.09
tB2GE-b	64.19	28.31	74.24	69.82	27.37	73.32	65.49
tB3GE	63.53	27.72	72.75	71.34	28.57	73.87	63.53

[a] Chemical shifts correspond to the carbon atom written in italics and underlined.

Elusive tB1GE-b and tB2GE-b have been recently identified by GC-MS [43], although their NMR characterization has not been reported. tB1GE-b, as in the case of tB2GE-a and tB3GE, shows a symmetry plane, so that a simple spectrum could be expected. Nevertheless, chemical shifts of H_2, H_a, and H_b were so close that signals corresponding to H_a and H_b were broad and appeared in the 3.60–3.68 ppm range, and the coupling constants could not be accurately determined. In the case of H_2, it appeared as an apparent quintuplet (J = 4.67 Hz) centered at 3.71 ppm. Concerning the tB1GE-b ^{13}C spectrum, it was recorded using an APT sequence that allowed the fast assignation of the signal at 28.68 ppm to the primary methyl carbon and the ones at 63.83 ppm and 71.12 ppm to the C_1 and C_3 secondary carbons and the C_2 tertiary carbon, respectively (see Appendix B). The long-range correlation of the signal at 1.24 ppm that corresponds to the CH₃ groups allowed the identification of a small signal at 74.75 ppm assigned to the quaternary carbon atom on the *tert*-butyl moiety.

Finally, the ^{1}H NMR spectrum for tB2GE-b showed four groups of signals in the glycerol skeleton and two singlets corresponding to the *tert*-butyl groups at 1.21 ppm and 1.19 ppm. The hydroxyl group appeared as a double doublet at 2.51 ppm (J = 3.78 Hz, J = 7.94 Hz) due to coupling with the diasterotopic H_3. This hydroxyl signal showed strong HSQC-TOCSY correlation with the carbon atom at 65.65 ppm that corresponded then to C_3 (Figure 4a). Once C_3 was assigned, the heteronuclear ^{1}H–^{13}C experiment combined with ^{13}C APT allowed easy assignation of C_1, C_2, H_1, and H_2 (Figure 4b). The hydrogen atom on the hydroxyl group presented a clear NOE effect with the hydrogen atoms on the *tert*-butyl group at 1.19 ppm (Figure 4c) that were hence assigned to the *tert*-butyl group on C_2. The long-range correlation in the HMBC spectrum (Figure 4d) allowed the identification of the quaternary carbon atoms.

The ^{1}H signals for H_2 and H_3 signals overlapped, making the resolution of the system difficult. As for H_1, two ^{1}H NMR signals were observed, the first centered at 3.41 ppm and the second at 3.34 ppm (Figure 5). The geminal coupling constant for H_{1a} and H_{1b} was 8.60 Hz, and they both coupled with H_2 with J = 4.30 Hz and J = 8.58 Hz, respectively, causing the triplet aspect of the signal at 3.34 ppm that indeed corresponded to a double doublet. The chemical shifts for H_2 and H_{3a} and H_{3b} were determined using the HSQC-TOCSY cross-signals with C_2 and C_3, respectively. The coupling constants for H_2 and H_3 needed to be determined using the spectrum simulation module in Topspin 3.6.2 and are gathered in Table 1.
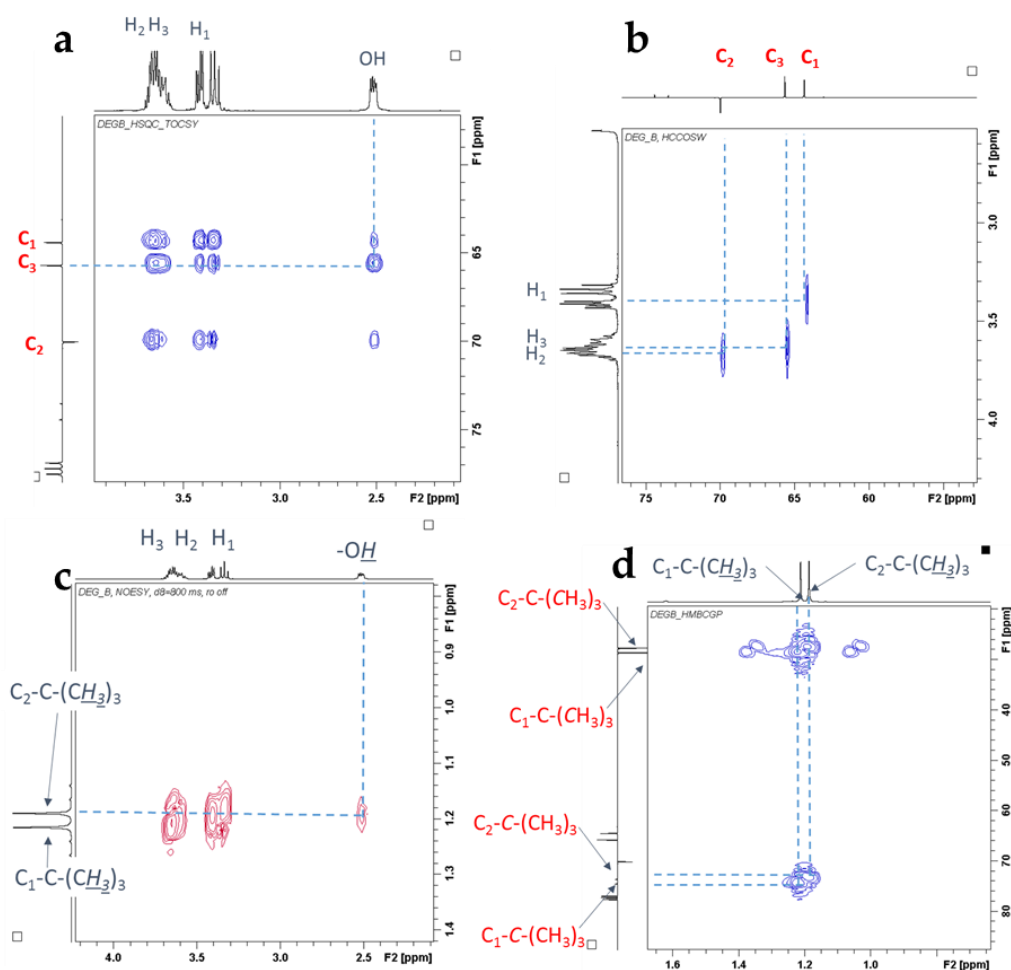
Figure 4. Details of the *t*B2GE-b spectra: (**a**) the HSQC-TOCSY spectrum, (**b**) the ^{1}H–^{13}C heteronuclear correlation, (**c**) the NOESY experiment, and (**d**) the HMBCGP experiment.
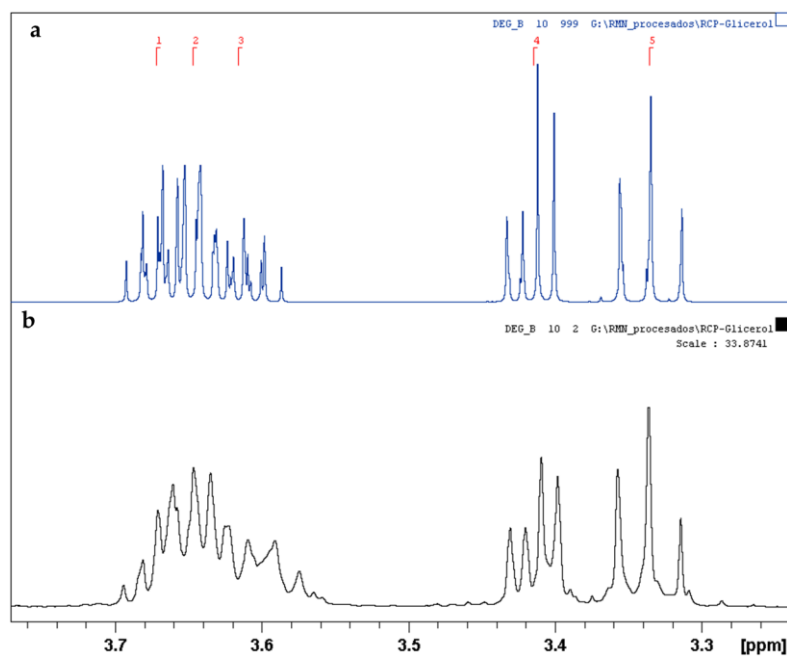

Figure 5. (**a**) Simulation of the *t*B2GE-b ^{1}H NMR spectrum using Topspin. (**b**) Detail of the *t*B2GE-b ^{1}H NMR spectrum.

2.2. Glycerol Tert-Butylation Monitoring through GC Analyses

Gas chromatography (GC) is the benchmark analytical technique for monitoring etherification reactions between glycerol and *tert*-butyl alcohol (TBA), although it presents several drawbacks. Polyols like glycerol have low vapor pressures that makes necessary the use of relatively harsh analysis conditions together with long analysis times that do not ensure the precise quantification of glycerol and, consequently, accurate mass balances. In addition, the complete derivatization by silylation of the reaction mixture is difficult and laborious and requires high quantities of specific reagents. Nevertheless, as shown in Figure 6, it allows the appropriate separation of the five *t*BGEs, glycerol, and the internal standard in ca. 20 min, although unreacted TBA cannot be quantified as it elutes with the solvent used to dilute the sample taken from the reaction mixture.
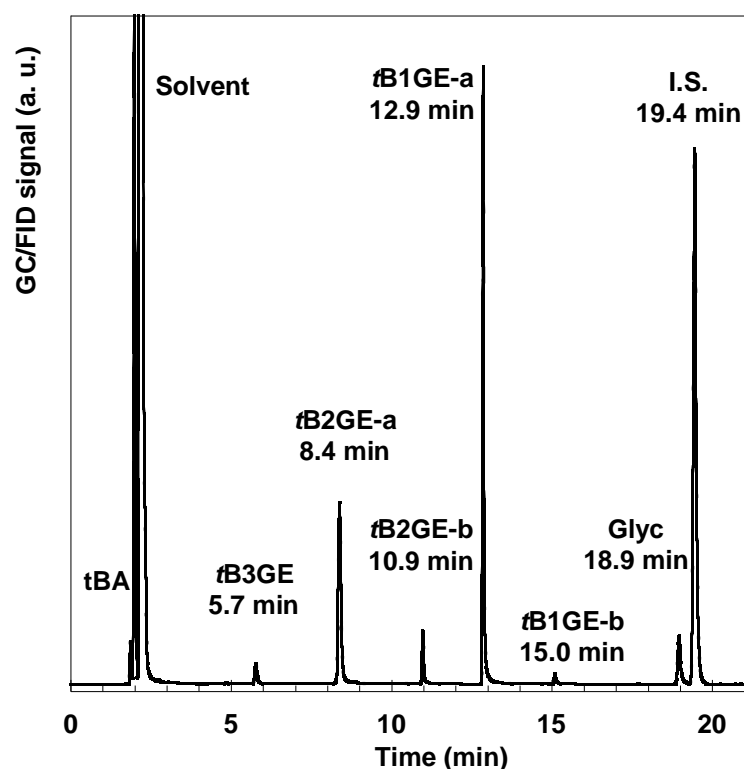

Figure 6. Typical GC-FID chromatogram of a *tert*-butylation mixture sample. Glyc stands for glycerol, and S.I. stands for internal standard.

Figure 7 shows the *t*BGE content of the reaction mixture expressed as molar fractions as a function of the glycerol conversion achieved after 24 h of *tert*-butylation reaction at temperatures between 70 and 110 °C, 8 wt.% PTSA, referred to the initial glycerol content and TBA/glycerol molar ratios within the 4:1–16:1 range. It can be observed that *t*B1GE-a and *t*B2GE-a were the main *tert*-butyl glycerol ethers produced. In addition, the *t*B1GE-a content was much higher than that of *t*B2GE-a, which only reached significant concentrations once the monoether was sufficiently abundant, in accordance to a reaction scheme in series. The formation of 1- and 1,3-ethers from the condensation of primary hydroxyl groups of glycerol to produce *t*B1GE-a and *t*B2GE-a was more probable against the formation of 2- and 1,2-ethers, *t*B1GE-b, and *t*B2GE-b [26]. Indeed, glycerol was a triol having double the number of primary than secondary hydroxyl groups. In addition, primary hydroxyls were preferred for *tert*-butylation due to steric effects because the *tert*-butyl group was a voluminous moiety. This explained in part the very low concentrations of the triether achieved, which was present in detectable amounts when the glycerol conversions reached values above ca. 0.75. Another reason was the thermodynamic limitations that appeared when TBA was used as the alkylating agent [18]. The *t*B1GE-b

and *t*B2GE-b contents were also very low. The evolution of the molar fractions suggested that *t*B1GE-b disappeared to form *t*B2GE-b and that this diether reacted to form the triether *t*B3GE, as indicated by arrows in Figure 7.
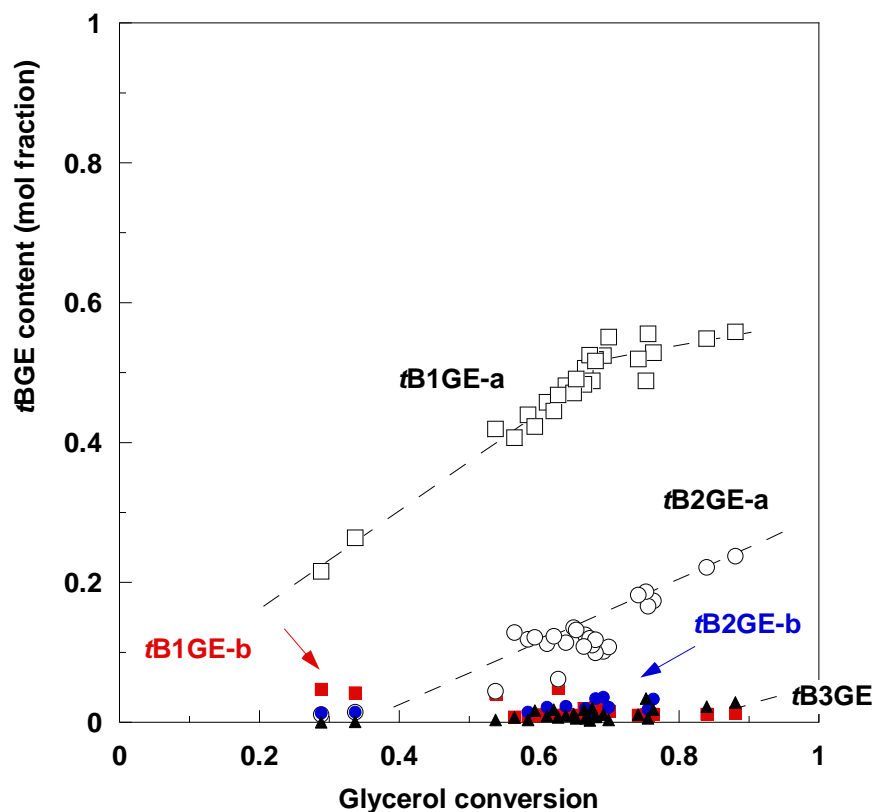

Figure 7. Molar fractions of the *t*BGEs according to GC-FID analyses of reaction mixtures after 24 h at 70–110 °C, 8 wt.% PTSA, referred to the initial glycerol content and TBA/glycerol molar ratios between 4:1 and 16:1.

2.3. Glycerol Tert-Butylation Monitoring through ^{1}H NMR Analyses

Given that the ^{1}H NMR signal was directly proportional to the amount of hydrogen atoms present in the sample, in principle, no calibration was required for the quantification of samples whose analysis required only 90 s. Initially, the ^{1}H NMR spectra of the isolated glycerol and the *t*B1GE-a, *t*B2GE-a, and *t*B3GE. *t*BGEs were superimposed (Figure 8a) in an attempt to find out a relation between the results of the integration of the different spectra regions and the molar fraction of each compound. However, the spectra of the reaction mixtures were slightly different from those corresponding to the isolated product superposition (Figure 8b). This was due to the differences in the solvent dielectric properties due to the presence of high amounts of TBA and glycerol in the reaction mixture. Hence, the spectra of the samples from the etherification reactions were much easier to interpret than those corresponding to the component superposition, which allowed the simplification of the quantitative analysis defining four integration regions (denoted as R_j, j = 1, 2, 3, 4) and assuming negligible the contributions of *t*B1GE-b and *t*B2GE-b. As for the rest of the compounds, their contributions to the several integration regions are gathered in Table 3. An obvious drawback of this procedure was that no distinction could be made between both monoethers and diethers.
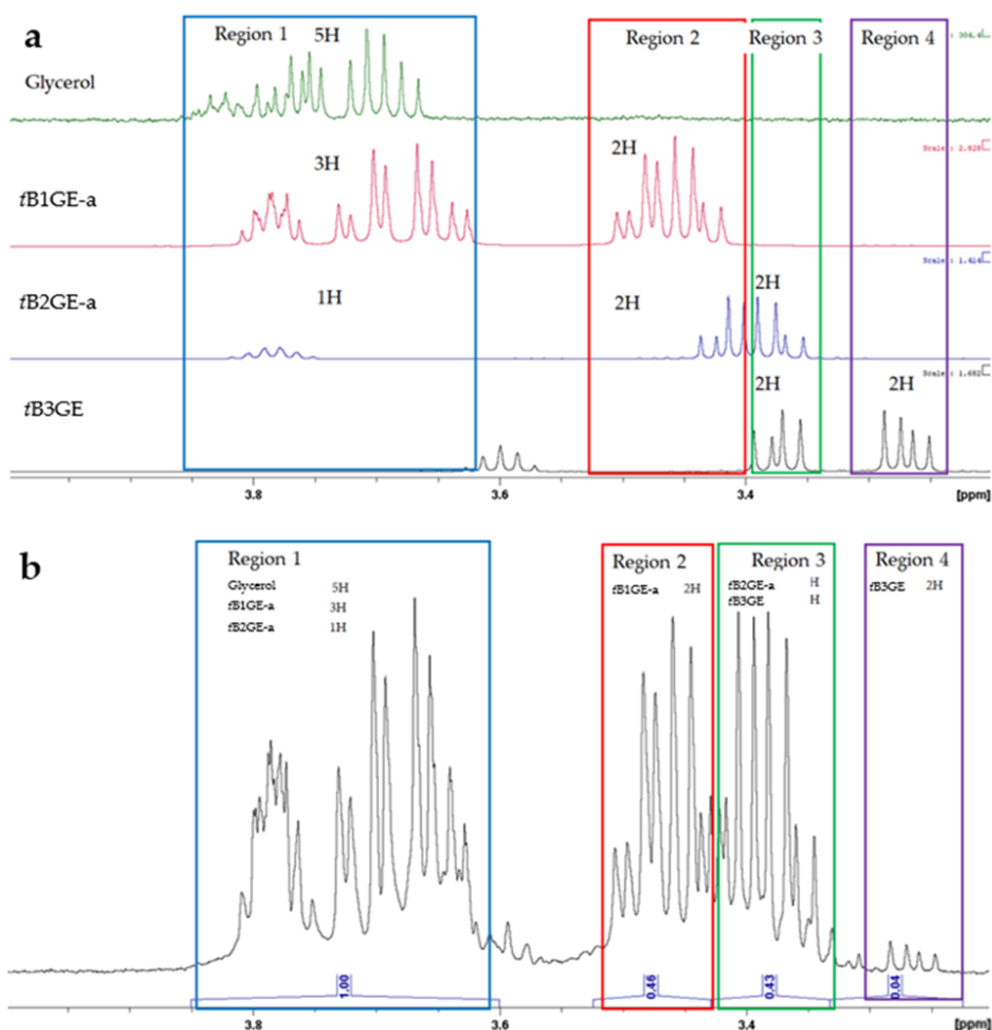
Figure 8. (**a**) Superimposed ^{1}H NMR spectra for glycerol, *t*B1GE-a, *t*B2GE-a, and *t*B3GE. (**b**) The ^{1}H NMR spectrum of a reaction sample.

Table 3. Contribution of the compounds indicated to the integration of the NMR spectra regions.

Region, R_j	δ (ppm)	Glycerol	*t*B1GE-a	*t*B2GE-a	*t*B3GE
1	3.850–3.604	5	3	1	-
2	3.524–3.429	-	2	-	-
3	3.429–3.333	-	-	4	2
4	3.333–3.225	-	-	-	2

Accordingly, the molar fractions of glycerol and the *t*BGEs were calculated from the values (n_i) given by Equations (1)–(6), which were proportional to the number of moles of each compound present in the sample. In these equations, IA_{Rj} (j = 1,2,3,4) are integration values corresponding to the region j according to Table 3. The conversion of glycerol (X_{Glyc}) and the *t*BGE selectivities (S_i) can be calculated according to Equations (5) and (6), respectively, considering that no products other than *t*BGEs and unreacted glycerol were present in the reaction mixture. Due to the abovementioned limitations of NMR analyses, in what follows, selectivities are reported for *t*B1GE and *t*B2GE that lump both monoethers and both diethers, respectively.

$$n_{t\text{B1GE}} = \frac{IA_{R2}}{2} \tag{1}$$

$$n_{t\text{B2GE}} = \frac{(IA_{R3} - IA_{R2})}{4} \tag{2}$$

$$n_{t\text{B3GE}} = IA_{R4} \tag{3}$$

$$n_{\text{Glyc}} = \frac{IA_{R1} - 3 \cdot n_{t\text{B1GE}} - n_{t\text{B2GE}}}{5} = \frac{(4 \cdot IA_{R1} - 6 \cdot IA_{R2} - IA_{R3} - IA_{R4})}{20} \tag{4}$$

$$X_{\text{Glyc}} = \frac{n_{t\text{B}_1\text{GE}} + n_{t\text{B}_2\text{GE}} + n_{t\text{B}_3\text{GE}}}{n_{\text{Glyc}} + n_{t\text{B}_1\text{GE}} + n_{t\text{B}_2\text{GE}} + n_{t\text{B}_3\text{GE}}} \tag{5}$$

$$S_i = \frac{n_i}{n_{t\text{B}_1\text{GE}} + n_{t\text{B}_2\text{GE}} + n_{t\text{B}_3\text{GE}}} \quad i = n_{t\text{B1GE}}, n_{t\text{B2GE}}, n_{t\text{B3GE}} \tag{6}$$

Figure 9 shows the relation between the selectivities to *tert*-butyl mono-, di-, and triethers of glycerol obtained, calculated from the results of the analyses performed by GC and ^{1}H NMR of the reaction samples. In general, a good agreement is observed; however, some samples led to larger discrepancies. The quantification of glycerol was identified as the main source of error, which reached ca. 5% and 7% for the NMR and GC analyses, respectively. In the case of the *t*BGEs, the errors were reduced to ca. 3% with both techniques. Higher errors could be associated to homogenization difficulties, particularly in samples with very low or very high glycerol conversions. In the first case, the high polarity and viscosity of glycerol complicated the sample manipulation. In the second case, the large difference in polarity between the reaction products, especially the di- and triethers, and that of the reactants led to the formation of micro-emulsions through phase segregation.
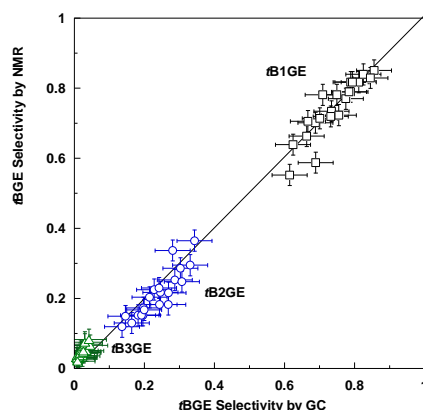

Figure 9. Selectivities to the *t*BGEs calculated from ^{1}H NMR and GC analyses.

Monitoring of the glycerol *tert*-butylation reactions through ^{1}H NMR has allowed illustrating the effects of some of the reaction conditions. In this regard, Figure 10 shows the influence on the glycerol conversion of the catalyst (PTSA) concentration after 24 h of reactions conducted at 70 °C and TBA/glycerol molar ratios of 4:1, 8:1, and 16:1. It can be seen that as expected, at a given TBA/glycerol ratio, the glycerol conversion increases at increasing PTSA concentration. For example, at the TBA/glycerol molar ratio of 4:1, the conversion increased from ca. 70% to 95% when the catalyst concentration passed from 8 wt.% to 32 wt.%. However, at a given catalyst content, the glycerol conversion decreased as the TBA/glycerol molar ratio increased. This was explained by the fact that the catalyst concentration was referred to the initial glycerol content of the reaction mixture. Therefore, the catalyst concentration over the total reaction volume decreased as the TBA/glycerol ratio increased due to the dilution caused by increasing amounts of TBA. For instance, when the catalyst concentration was fixed at 32 wt.% referred to the glycerol amount, the

overall catalyst concentration decreased from 6.4 wt.% to 1.9 wt.% and finally 1.0% when the TBA/glycerol ratio increased from 4:1 to 8:1 and 16:1, respectively.
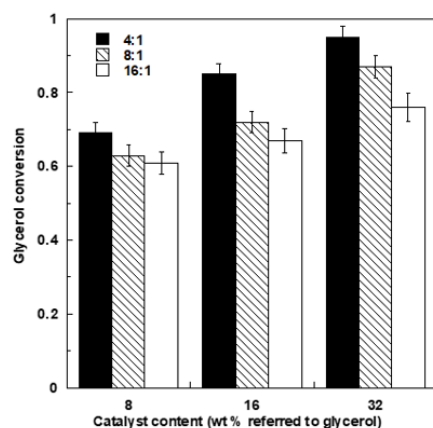

Figure 10. Glycerol conversion after 24 h of reaction as a function of the catalyst content.

Figure 11 shows the *t*BGE selectivities for the conversion points included in Figure 7. It can be seen that the selectivities were dictated by their own reaction progress, that is, the glycerol conversion. The catalyst content and TBA/glycerol ratio affected the conversion that could be achieved in a given reaction time, in this case, 24 h, but did not seem to influence the selectivity. In other words, the highest glycerol conversions attained corresponded to the reactions performed at the lowest TBA/glycerol ratio (4:1) and the highest PTSA concentration (32 wt.% referred to the initial glycerol amount) considered. High glycerol conversions were necessary to obtain the highest possible di- and triether selectivities. The first ones reached values of ca. 35% at their highest, whereas in the conditions of the present study, maximum *t*B3GE selectivities of ca. 8% were obtained. As concerns the monoethers, maximum conversions were obtained at the lowest glycerol conversion. In accordance with the in-series scheme that followed the *tert*-butylation reaction, the first products were proportionally more abundant at short reaction times (in batch processes), when they had little opportunity of being converted into higher ethers. As for the temperature, an effect similar to the rest of reaction variables was found, having a positive influence on the glycerol conversion but not affecting the *t*BGE selectivities.
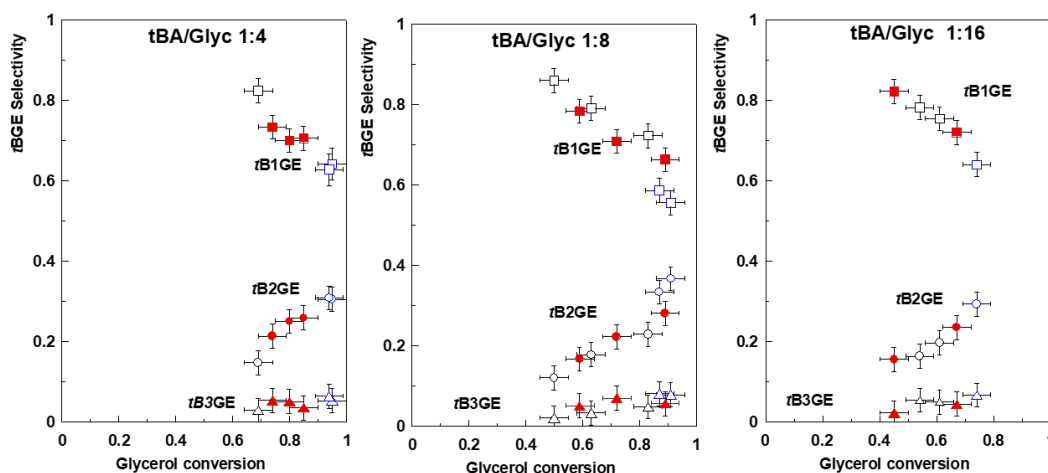

Figure 11. *t*BGE selectivities for glycerol etherification reaction conducted at TBA/glycerol molar ratios of 4:1 (**left**), 8:1 (**center**), and 16:1 (**right**). Catalyst (PSA) concentrations referred to the glycerol content were: 8 wt.% (open black symbols), 16 wt.% (filled red symbols), and 32 wt.% (open blue symbols).

2.4. Etherification of the Tert-Butyl Glycerol Monoether

With the purpose of increasing the yield of the higher *t*BGEs, the *tert*-butylation reaction was carried out starting from *t*B1GE instead of glycerol as indicated in Section 3.2. Figure 12 shows the evolution with reaction time of the *t*BGE molar fractions monitored through ^{1}H NMR (Figure 12a) and GC (Figure 12b). It was clear that the monoether converted into the diether without having a significant impact on the triether concentration. After the fifth day of reaction, the monoether conversion reached 38%; at that time, a new charge of TBA and catalyst was performed, aiming at further converting the monoether. The conversion increased up to 56% after two additional days of reaction. The GC analyses allowed distinguishing between both diethers, and the obtained results (Figure 12b) suggested that the triether was mainly formed from *t*B2GE-b. This seemed reasonable in view of the much stronger steric hindrance that would entail its formation from *t*B2GE-a. However, *t*B2GE-b was much less abundant than *t*B2GE-a, that is, the diether with both glycerol primary hydroxyl groups etherified. This showed that there were intrinsic difficulties in obtaining high selectivities to the *tert*-butyl glycerol triether through the homogeneously acid-catalyzed *tert*-butylation of glycerol with TBA.
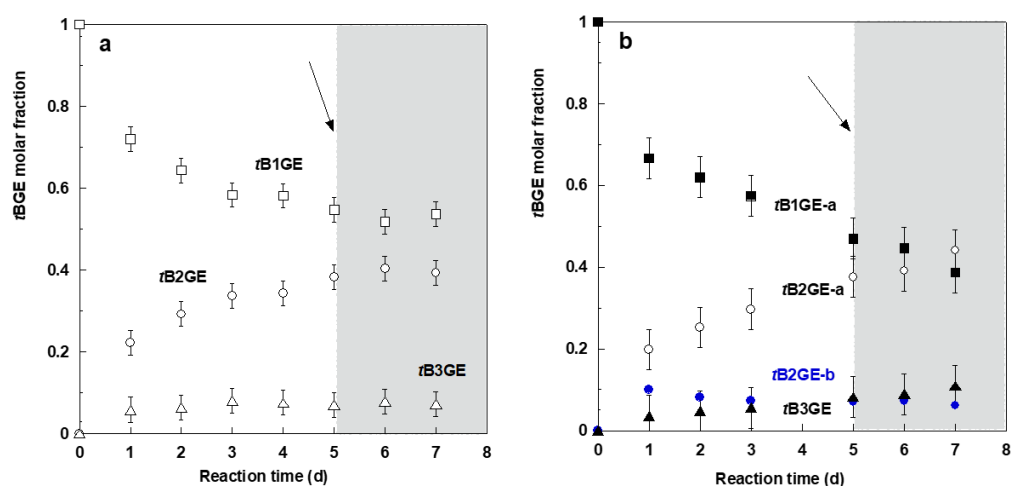

Figure 12. Evolution of *t*BGE concentration during the etherification with TBA of the *tert*-butyl glycerol monoether as monitored by (**a**) ^{1}H NMR and (**b**) GC. The arrows indicate the addition of a new charge of TBA and catalyst.

3. Materials and Methods

3.1. Materials and Analytical Techniques

tert-Butanol (TBA), anhydrous glycerol (99.5%), and 1,3,5-trimethoxybenzene (as the internal standard) were purchased from Acros Organics (Fairlawn, NJ, USA) *p*-Toluenesulfonic acid (PTSA) used as the homogeneous catalyst was purchased from Panreac S.L. (Darmstadt, Germany) CDCl$_3$ was purchased from Carlo-Erba (Val de Reuill, France) and used as received.

The attenuated total reflectance (ATR) infrared (IR) spectra were recorded on an Avatar 360 FT-IR spectrometer (ThermoFisher Scientific, Walthman, MA, USA). The gas chromatography (GC) analyses were performed on a Shimadzu gas chromatograph equipped (Kyoto, Tapan) with a flame ionization detector (FID) and a DB-23 (30 m, 0.32 mm ID, 0.25 μm) column. During the analyses, the oven temperature was kept for 10 min at 90 °C, then it was raised from 90 to 150 °C at a rate of 25 °C/min, and finally, it was maintained for 8 min at 150 °C. The samples for the GC analysis were prepared from 0.040 g of the reaction mixture that were diluted with 2.5 mL of a 2 g/L solution of 1,3,5-trimetoxybenzene in acetonitrile.

The nuclear magnetic resonance (NMR) analyses were performed on a Bruker Ascend 400 spectrometer (Rheinstetten, Germany) operated at 400 MHz and equipped with a PA

BBO 5 mm probe. All ^{1}H and ^{13}C chemical shifts were reported using the δ scale and were referenced to the residual signal of CHCl$_3$ at 7.26 ppm and that of *CDCl$_3$* at 77.16. The pulse programs were the previously installed *zg30* for ^{1}H with 16 scans. CDCl$_3$ was the solvent of choice after discarding DMSO-d_6 and CD$_3$OD due to the overlapping of residual signals from CD$_2$HOD and H$_2$O, respectively, from those of the reaction products.

3.2. Tert-Butylation Reactions

Glycerol etherification reactions were performed in a 100 mL stainless steel stirred autoclave at 30 bar, TBA/glycerol molar ratios ranging between 4:1 and 16:1, catalyst concentrations of 8–32 wt.% PTSA referred to the glycerol loaded into the reactor, and temperatures within 70–90 °C. The samples were withdrawn from the reactors during the course of the reaction by means of the appropriate recirculating valves to maintain the pressure and agitation conditions.

An experiment was carried out using 1.5 g of the monoethers (*t*B1GEs), 10 g TBA and 0.24 g glycerol (TBA/glycerol molar ratio of 13.5:1), 70 °C, and 16 wt.% of PTSA catalyst referred to the *t*B1GEs. After five days of reactions, a new charge into the reactor of 10 g TBA and 0.24 g glycerol was carried out.

3.3. Isolation of the Tert-Butyl Ethers

In order to obtain the *t*BGEs for the NMR identification, a glycerol etherification reaction was conducted on the stainless steel autoclave at 90 °C and 30 bar with a TBA/glycerol molar ratio of 4:1 and 8 wt.% PTSA referred to the glycerol loaded into the reactor. After 24 h of reaction, the resulting mixture was concentrated in a rotary evaporator to remove the unreacted alcohol. Afterward, ca. 17 g of the *t*BGE/glycerol mixture were charged into a chromatography column using M60 silica as stationary phase. *t*B3GE, *t*B2GE-a, and *t*B2GE-b (see Figure 1) were separated using hexane/ethyl acetate (9:1) as the mobile phase, as reported by González et al. [42]. On the other hand, the *t*B1GE-a and *t*B1GE-b monoethers were eluted using a hexane/ethyl acetate (1:9) mixture.

4. Conclusions

Glycerol *tert*-butylation is a complex reaction leading to the formation of five glycerol *tert*-butyl ethers (*t*BGEs). All of them have practical interest: the monoethers as surfactants and components of cosmetics and pharmaceuticals and the di- and triethers as fuel additives. In order to suitably monitor the progress of the reaction between glycerol and *tert*-butanol (TBA), a method based on ^{1}H NMR analyses was developed in the present work that allowed for the quantification of unreacted glycerol and the *t*BGEs in only 90 s without the need for equipment calibration. These features are clear advantages compared with conventional GC analyses when fast, almost real-time, monitoring of the reaction is required. In contrast, the method was not able to distinguish between both monoether and both diether isomers, which were lumped into two groups of reaction products. For that reason, it was necessary to combine ^{1}H NMR and GC analyses to obtain a complete characterization of the reaction mixture.

The set of results available for the development of the analytical methods provided information of interest as concerns the formation of higher ethers. Glycerol *tert*-butylation is a consecutive reaction in which primarily formed monoethers lead to diethers that are finally converted into the triether. According to our results, the triether seemed to be formed from *t*B2GE-b instead of *t*B2GE-a due to easier access of the third *tert*-butyl moiety to a primary carbon atom than to a secondary one. However, the fact that *t*B2GE-a was much easier to form than *t*B2GE-b due to the higher reactivity of primary hydroxyls compared with the secondary ones, the double number of primary as compared with secondary hydroxyls present in glycerol, and steric effects explained the difficulties in forming the *tert*-butyl glycerol triether through this synthetic route.
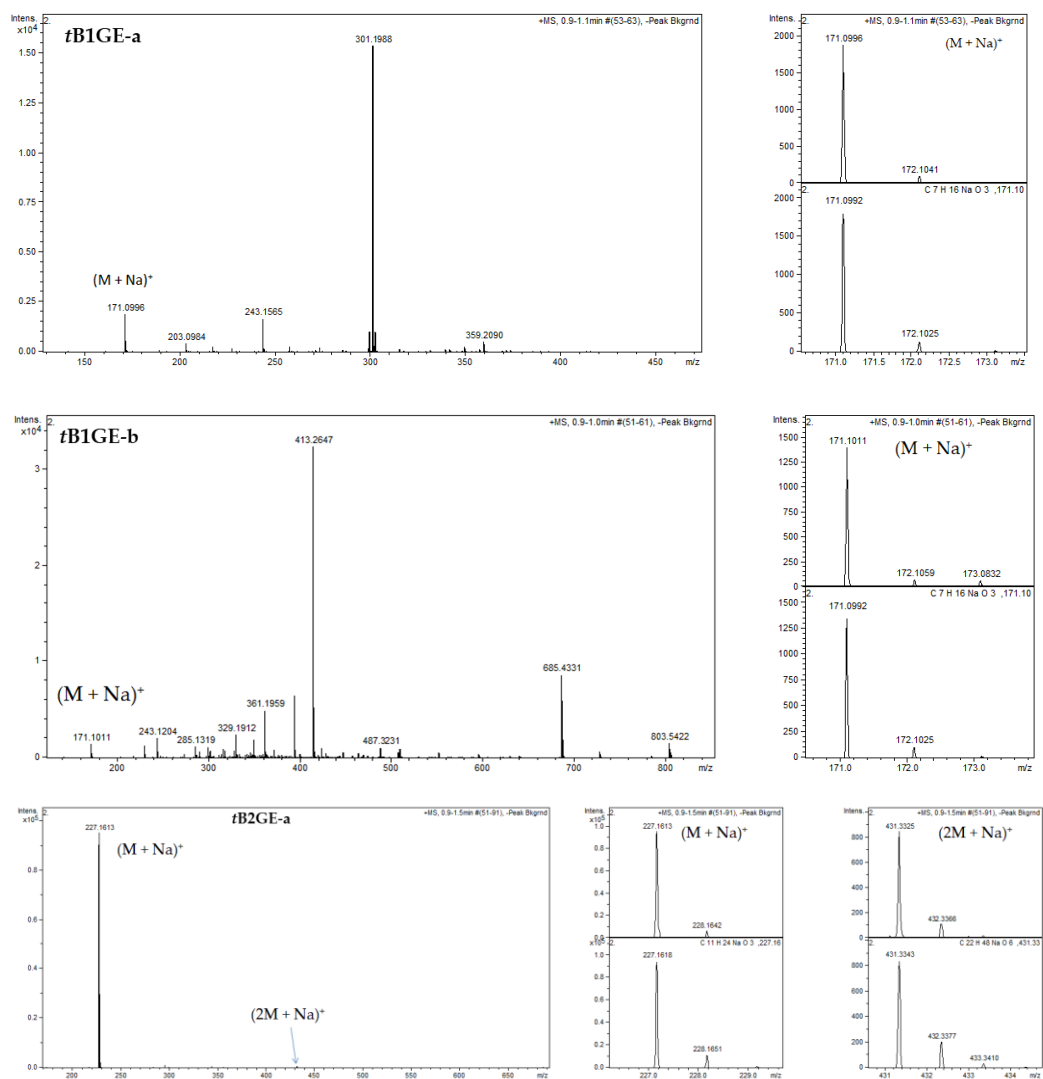
Appendix A

Figure A1. *Cont*.

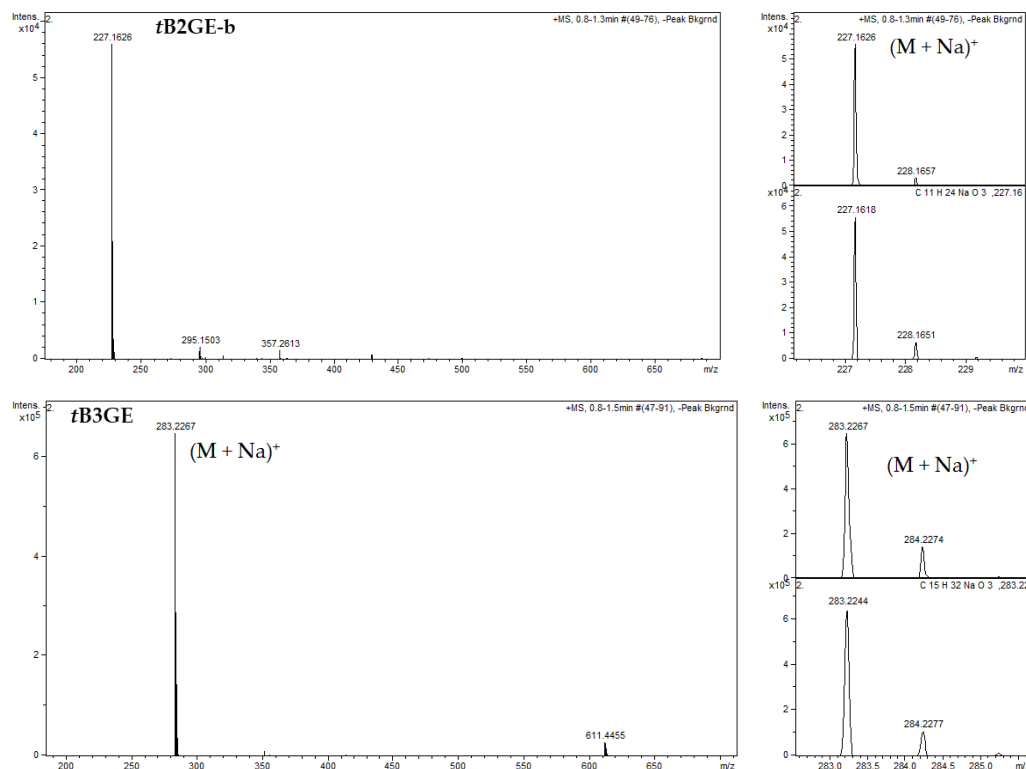**Figure A1.** MS-ESI$^+$ spectra of *tert*-butyl ethers of glycerol.
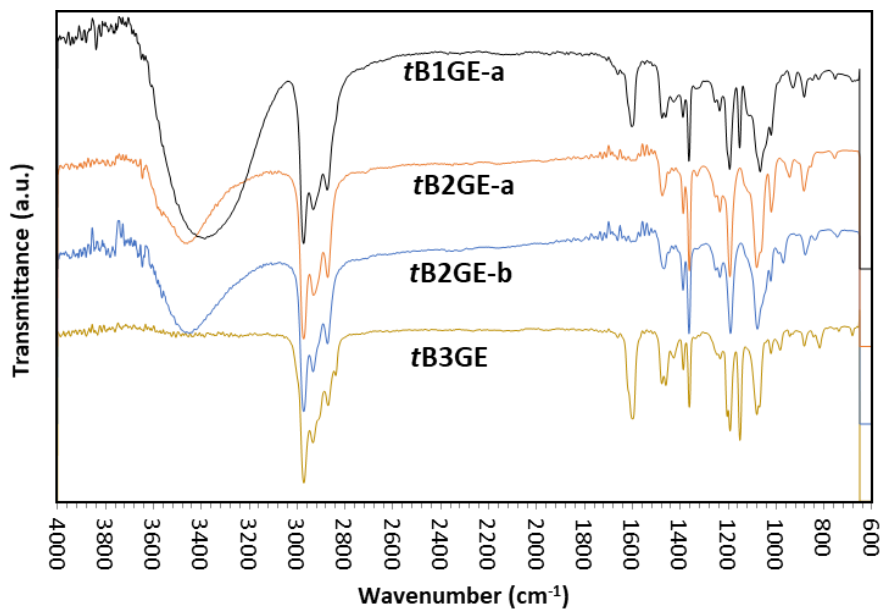
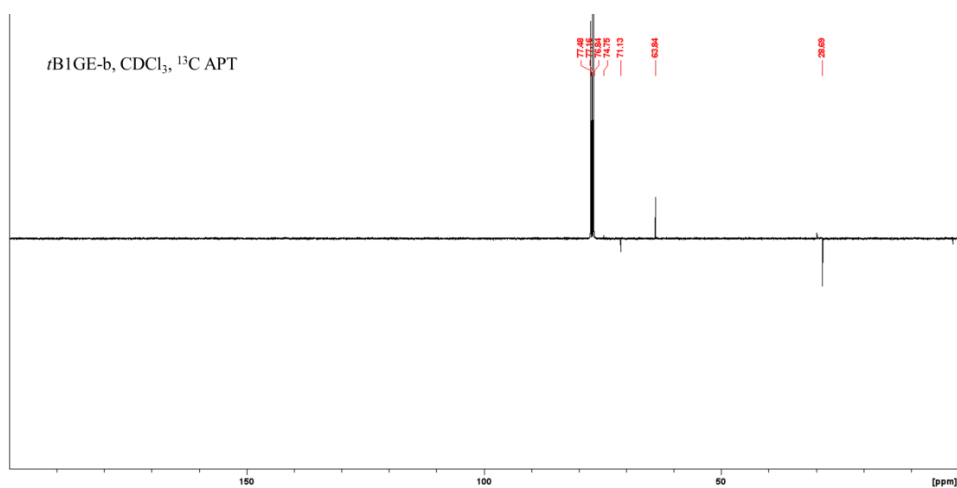**Figure A2.** FTIR spectra of *tert*-butyl ethers of glycerol.

Appendix B

*t*B1GE-a, CDCl₃, ¹H

ethyl acetate

Figure A3. The ¹H NMR spectrum of *t*B1GE-a in CDCl₃.

*t*B1GE-a, CDCl₃, ¹³C APT

Figure A4. The ¹³C APT NMR spectrum of *t*B1GE-a in CDCl₃.

*t*B1GE-b, CDCl₃, ¹H

Figure A5. The ¹H NMR spectrum of *t*B1GE-b in CDCl₃.

Figure A6. The ^{13}C APT NMR spectrum of *t*B1GE-b in CDCl$_3$.
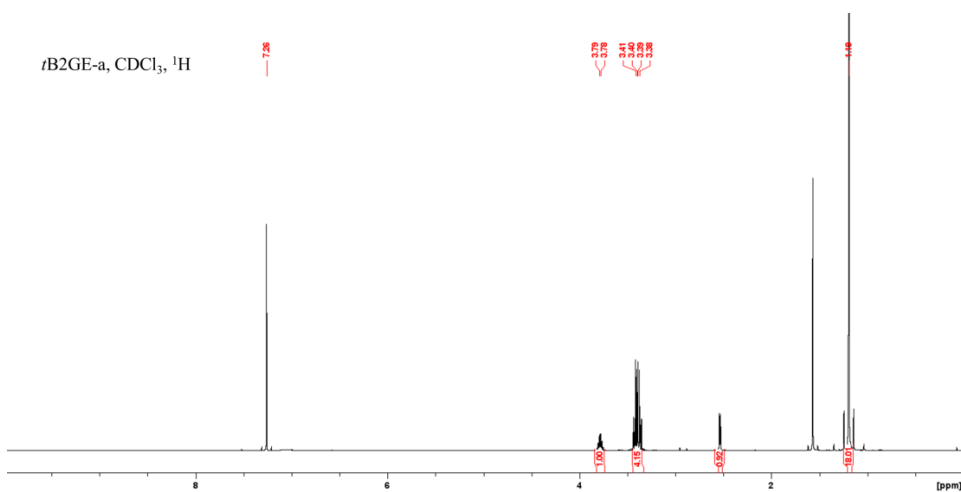
Figure A7. The ^{1}H NMR spectrum of *t*B2GE-a in CDCl$_3$.
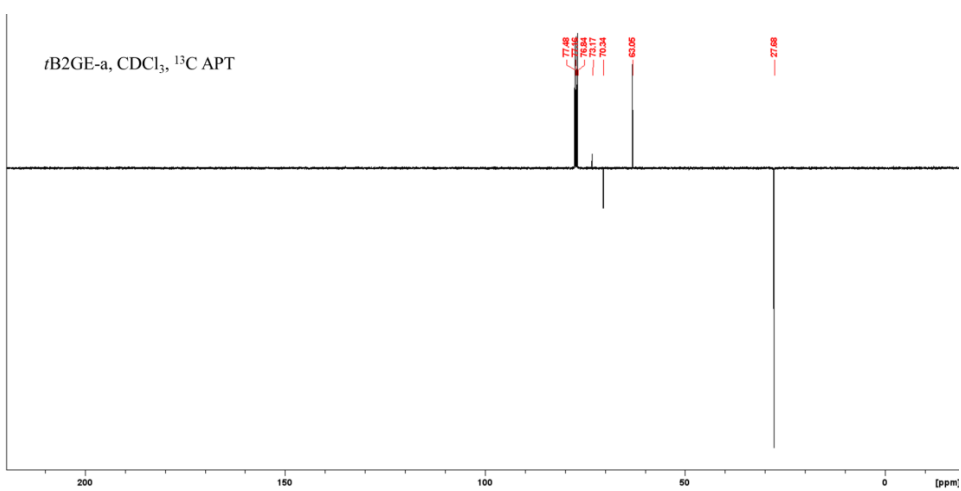
Figure A8. The ^{13}C APT NMR spectrum of *t*B2GE-a in CDCl$_3$.

Figure A9. The ^{1}H NMR spectrum of *t*B2GE-b in CDCl$_3$.

Figure A10. The ^{13}C APT NMR spectrum of *t*B2GE-b in CDCl$_3$.

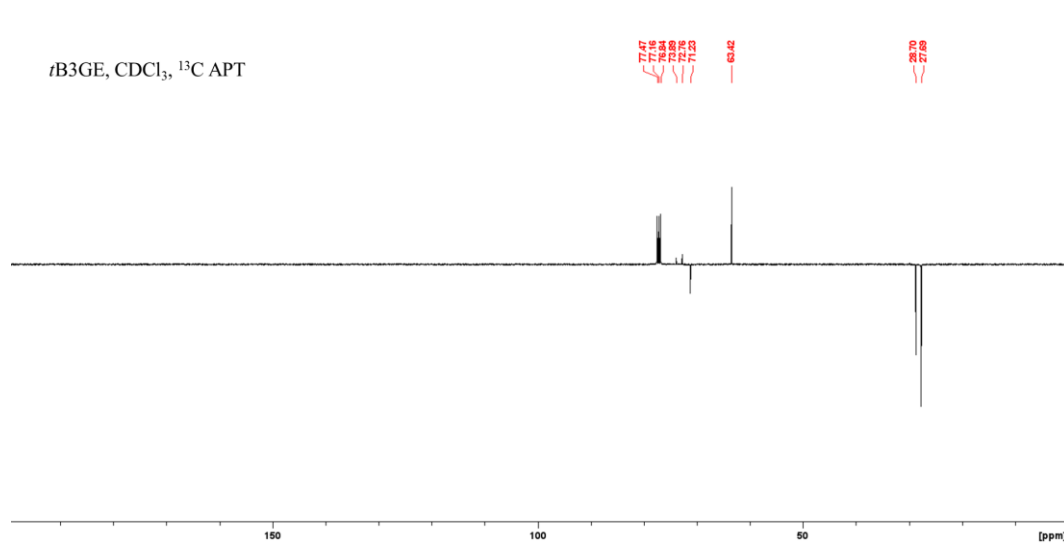**Figure A11.** The ^{1}H NMR spectrum of *t*B3GE in CDCl$_3$.

*t*B3GE, CDCl₃, ¹³C APT

Figure A12. The ¹³C APT NMR spectrum of *t*B3GE in CDCl₃.

References

1. ChemAnalyst. Glycerine Market Analysis. Available online: https://www.chemanalyst.com/industry-report/glycerine-market-635 (accessed on 7 August 2023).
2. International Energy Agency. *Renewables 2022. Analysis and Forecast to 2027*; International Energy Agency: Paris, France, 2022.
3. Morais Lima, P.J.; da Silva, R.M.; Chaves Girão Neto, C.A.; Câmara Gomes e Silva, N.; da Silva Souza, J.E.; Nunes, Y.L.; Sousa dos Santos, J.C. An overview on the conversion of glycerol to value-added products via chemical and biochemical routes. *Biotechnol. Appl. Biochem.* **2022**, *69*, 2794–2818. [CrossRef] [PubMed]
4. Checa, M.; Nogales-Delgado, S.; Montes, V.; Encinar, J.M. Recent Advances in Glycerol Catalytic Valorization: A Review. *Catalysts* **2020**, *10*, 1279. [CrossRef]
5. Pirzadi, Z.; Meshkani, F. From glycerol production to its value-added uses: A critical review. *Fuel* **2022**, *329*, 125044. [CrossRef]
6. Kaur, J.; Sarma, A.K.; Jha, M.K.; Gera, P. Valorisation of crude glycerol to value-added products: Perspectives of process technology, economics and environmental issues. *Biotechnol. Rep.* **2020**, *27*, e00487. [CrossRef] [PubMed]
7. Gujar, J.P.; Modhera, B. A review on catalytic conversion of biodiesel derivative glycerol to bio-olefins. *Mater. Today Proc.* **2023**, *72*, 2723–2730. [CrossRef]
8. Zhang, J.; Wang, Y.; Muldoon, V.L.; Deng, S. Crude Glycerol and glycerol as fuel and fuel additives in combustion applications. *Renew. Sust. Energ. Rev.* **2022**, *159*, 112206. [CrossRef]
9. Liu, Y.; Zhong, B.; Lawal, A. Recovery and utilization of crude glycerol, a biodiesel byproduct. *RSC Adv.* **2022**, *12*, 27997. [CrossRef]
10. Cornejo, A.; Barrio, I.; Campoy, M.; Lázaro, J.; Navarrete, B. Oxygenated fuel additives from glycerol valorization. Main production pathways and effects on fuel properties and engine performance: A critical review. *Renew. Sust. Energ. Rev.* **2017**, *79*, 1400–1413. [CrossRef]
11. Olson, A.L.; Tunér, M.; Verhelst, S. A concise review of glycerol derivatives for use as fuel additives. *Heliyon* **2023**, *9*, e13041. [CrossRef]
12. Queste, S.; Boudin, P.; Touraud, D.; Kunz, W.; Aubry, J.-M. Short chain glycerol 1-monoethers—A new class of solvo-surfactants. *Green Chem.* **2006**, *8*, 822–830. [CrossRef]
13. Gu, Y.; Azzouzi, A.; Pouilloux, Y.; Jérôme, F.; Barrault, J. Hetrogeneously catalyzed etherification of glycerol: New pathways for transformation of glycerol to more valuable chemicals. *Green Chem.* **2008**, *10*, 164–167. [CrossRef]
14. Sutter, M.; Da Silva, E.; Duguet, N.; Raoul, Y.; Métay, E.; Lemaire, M. Glycerol Ether Synthesis: A Bench Test for Green Chemistry Concepts and Technologies. *Chem. Rev.* **2015**, *115*, 8609–8651. [CrossRef] [PubMed]
15. Palanychamy, P.; Lim, S.; Yap, Y.H.; Leong, L.K. Critical Review of the Various Reaction Mechanisms for Glycerol Etherification. *Catalysts* **2022**, *12*, 1487. [CrossRef]
16. Behr, A.; Obendorf, L. Development of a Process for the Acid-Catalyzed Etherification of Glycerine and Isobutane Forming Glycerine Tertiary Butyl Ethers. *Eng. Life Sci.* **2002**, *2*, 179–208. [CrossRef]
17. Liu, J.; Yang, B. Liquid–Liquid–Solid Mass Transfer and Phase Behavior of Heterogeneous Etherification of Glycerol with Isobutene. *AIChE J.* **2018**, *64*, 2526–2535. [CrossRef]

18. Dominguez, C.M.; Romero, A.; Santos, A. Improved Etherification of Glycerol with *Tert*-Butyl Alcohol by the Addition of Dibutyl Ether as Solvent. *Catalysts* **2019**, *9*, 378. [CrossRef]

19. Klepáčová, K.; Mravec, D.; Bajus, M. *tert*-Butylation of glycerol catalysed by ion-exchange resins. *Appl. Catal. A Gen.* **2005**, *294*, 141–147. [CrossRef]

20. Melero, J.A.; Vicente, G.; Morales, G.; Paniagua, M.; Moreno, J.M.; Roldán, R.; Ezquerro, A.; Pérez, C. Acid-catalyzed etherification of bio-glycerol and isobutylene over sulfonic mesostructured silicas. *Appl. Catal. A Gen.* **2008**, *346*, 44–51. [CrossRef]

21. Zhao, W.; Yang, B.; Yi, C.; Lei, Z.; Xu, J. Etherification of Glycerol with Isobutylene to Produce Oxygenate Additive Using Sulfonated Peanut Shell Catalyst. *Ind. Eng. Chem. Res.* **2010**, *49*, 12399–12404. [CrossRef]

22. Zhao, W.; Yi, C.; Yang, B.; Hu, J.; Huang, X. Etherification of glycerol and isobutylene catalyzed over rare earth modified Hβ-zeolite. *Fuel Process. Technol.* **2013**, *112*, 70–75. [CrossRef]

23. González, M.D.; Salagre, P.; Taboada, E.; Llorca, J.; Cesteros, Y. Microwave-assisted synthesis of sulfonic acid-functionalized microporous materials for the catalytic etherification of glycerol with isobutene. *Green Chem.* **2013**, *15*, 2230–2239. [CrossRef]

24. González, M.D.; Salagre, P.; Mokaya, R.; Cesteros, Y. Tuning the acidic and textural properties of ordered mesoporous silicas for their application as catalysts in the etherification of glycerol with isobutene. *Catal. Today* **2014**, *227*, 171–178. [CrossRef]

25. Bozkurt, Ö.D.; Bağlar, N.; Çelebi, S.; Uzun, A. Screening of solid acid catalysts for etherification of glycerol with isobutene under identical conditions. *Catal. Today* **2020**, *357*, 483–494. [CrossRef]

26. Klepáčová, K.; Mravec, D.; Bajus, M. Etherification of Glycerol with *tert*-Butyl Alcohol Catalysed by Ion-Exchange Resins. *Chem. Pap.* **2006**, *60*, 224–230. [CrossRef]

27. Frusteri, F.; Arena, F.; Bonura, G.; Cannilla, C.; Spadaro, L.; Di Blasi, O. Catalytic etherification of glycerol by *tert*-butyl alcohol to produce oxygenated additives for diesel fuel. *Appl. Catal. A Gen.* **2009**, *367*, 77–83. [CrossRef]

28. Pico, M.P.; Romero, A.; Rodríguez, S.; Santos, A. Etherification of Glycerol by *tert*-Butyl Alcohol: Kinetic Model. *Ind. Eng. Chem. Res.* **2012**, *51*, 9500–9509. [CrossRef]

29. Celdeira, P.A.; Gonçalves, M.; Figueiredo, F.C.A.; Dal Bosco, S.M.; Mandelli, D.; Carvalho, W.A. Sulfonated niobia and pillared clay as catalysts in etherification reaction of glycerol. *Appl. Catal. A Gen.* **2014**, *478*, 98–106. [CrossRef]

30. Gonçalves, M.; Soler, F.C.; Isoda, N.; Carvalho, W.A.; Mandelli, D.; Sepúlveda, J. Glycerol conversion into value-added products in presence of a green recyclable catalyst: Acid black carbon obtained from coffee ground wastes. *J. Taiwan Inst. Chem. Eng.* **2016**, *60*, 294–301. [CrossRef]

31. Srinivas, M.; Raveendra, G.; Parameswaram, G.; Sai Prasad, P.S.; Lingaiah, N. Cesium exchanged tungstophosphoric acid supported on tin oxide: An efficient solid acid catalyst for etherification of glycerol with *tert*-butanol to synthesize biofuel additives. *J. Mol. Catal. A Chem.* **2016**, *413*, 7–14. [CrossRef]

32. Estevez, R.; López, M.I.; Jiménez-Sanchidrián, C.; Luna, D.; Romero-Salguero, F.J.; Bautista, F.M. Etherification of glycerol with *tert*-butyl alcohol over sulfonated hybrid silicas. *Appl. Catal. A Gen.* **2016**, *526*, 155–163. [CrossRef]

33. Melero, J.A.; Vicente, G.; Morales, G.; Paniagua, M.; Bustamante, J. Oxygenated Compounds Derived from Glycerol for Biodiesel Formulation: Influence on EN 14214 Quality Parameters. *Fuel* **2010**, *89*, 2011–2018. [CrossRef]

34. Lee, H.J.; Seung, D.; Jung, K.S.; Kim, H.; Filimonov, I.N. Etherification of glycerol by isobutylene: Tuning the product composition. *Appl. Catal. A Gen.* **2010**, *390*, 235–244. [CrossRef]

35. Altaner, C.M.; Saake, B. Quantification of the chemical composition of lignocellulosics by solution ^{1}H NMR spectroscopy of acid hydrolysates. *Cellulose* **2016**, *23*, 1003–1010. [CrossRef]

36. De Souza, A.C.; Rietkerk, T.; Selin, C.G.M.; Lankhorst, P.P. A robust and universal NMR method for the compositional analysis of polysaccharides. *Carbohydr. Polym.* **2013**, *95*, 657–663. [CrossRef] [PubMed]

37. Mittal, A.; Scott, G.M.; Amidon, T.E.; Kiemle, D.J.; Stipanovic, A.J. Quantitative analysis of sugars in wood hydrolyzates with ^{1}H NMR during the autohydrolysis of hardwoods. *Bioresour. Technol.* **2009**, *100*, 6398–6406. [CrossRef] [PubMed]

38. Cornejo, A.; Alegria-Dallo, I.; García-Yoldi, Í.; Sarobe, Í.; Sánchez, D.; Otazu, E.; Funcia, I.; Gil, M.J.; Martínez-Merino, V. Pretreatment and enzymatic hydrolysis for the efficient production of glucose and furfural from wheat straw, pine and poplar chips. *Bioresour. Technol.* **2019**, *288*, 121583. [CrossRef]

39. Cornejo, A.; Bimbela, F.; Moreira, R.; Hablich, K.; García-Yoldi, Í.; Maisterra, M.; Portugal, A.; Gandía, L.M.; Martínez-Merino, V. Production of Aromatic Compounds by Catalytic Depolymerization of Technical and Downstream Biorefinery Lignins. *Biomolecules* **2020**, *10*, 1338. [CrossRef]

40. Talavera-Prieto, N.M.C.; Ferreira, A.G.M.; Moreira, R.J.; Portugal, A.T.G. Monitoring of the Transesterification Reaction by Continuous Off-Line Density Measurements. *Fuel* **2020**, *264*, 116877. [CrossRef]

41. Kundu, R.; De, S. Characterization and analysis of the triglyceride transesterification process. *Biomass Convers. Biorefinery* **2023**, *13*, 4933–4948. [CrossRef]

42. González, M.D.; Cesteros, Y.; Llorca, J.; Salagre, P. Boosted selectivity toward high glycerol tertiary butyl ethers by microwave-assisted sulfonic acid-functionalization of SBA-15 and beta zeolite. *J. Catal.* **2012**, *290*, 202–209. [CrossRef]

43. Veiga, P.M.; Dias, A.G.; Henriques, C.A. Identification of Ethyl and t-Butyl Glyceryl Ethers Using Gas Chromatography Coupled with Mass Spectrometry. *J. Braz. Chem. Soc.* **2018**, *29*, 1328–1335. [CrossRef]

44. Jamróz, M.E.; Jarosz, M.; Witowska-Jarosz, J.; Bednarek, E.; Tecza, W.; Jamróz, M.H.; Dobrowolski, J.C.; Kijeński, J. Mono-, Di-, and Tri-Tert-Butyl Ethers of Glycerol: A Molecular Spectroscopic Study. *Spectroc. Acta Part A Mol. Biomol. Spectr.* **2007**, *67*, 980–988. [CrossRef] [PubMed]

45. Reich, H.J. WinDNMR:Dynamic NMR Spectra for Windows. *J. Chem. Educ.* **1995**, *72*, 1086. [CrossRef]